Available online at www.keaipublishing.com/en/journals/journal-of-magnesium-and-alloys/

ScienceDirect

Journal of Magnesium and Alloys xxx (xxxx) xxx

www.elsevier.com/locate/jma

Full Length Article

Enhanced corrosion resistance of AZ31 magnesium alloys through the use of high-purity raw magnesium

Xin-Yu Peng, De-Gang Xie*, Long-Qi Bai, Zhang Liu, Zhi-Wei Shan*

State Key Laboratory for Mechanical Behavior of Materials, Engineering Research Center for Magnesium-based New Materials, Center for Advancing Materials Performance from the Nanoscale (CAMP-Nano), Xi'an Jiaotong University, Xi'an 710049, PR China

Received 9 August 2024; received in revised form 19 October 2024; accepted 30 October 2024
Available online xxx

Abstract

Poor corrosion resistance is a critical barrier to the widespread application of magnesium alloys. Statistically, the literature reported that approximately 70 % of as-cast AZ31 magnesium alloys exhibit corrosion rates exceeding 1 mm $\cdot y^{-1}$ in 3.5 wt.% NaCl solution, which is unacceptable for industrial use. Furthermore, there is a considerable discrepancy in the corrosion rates reported by different studies (as-cast alloys ranging from 0.4 to 215 mm $\cdot y^{-1}$). These phenomena may be attributed to the uncontrollable content of impurity elements in commercial magnesium alloys, which fluctuate widely between batches. In the present work, we prepared as-cast AZ31 magnesium alloys with different impurity contents using two different purities of raw magnesium (Mg-99.9% and Mg-99.99%). The impact of impurity contents on the corrosion resistance of AZ31 magnesium alloys was then analyzed. The AZ31 magnesium alloy prepared with 99.99% raw magnesium showed superior corrosion resistance compared with that prepared with 99.9% raw magnesium, with a reduction in corrosion rate by approximately 98 % and a decrease in the fluctuation range of corrosion rate by 91 %. Thus, enhancing the purity of raw magnesium is an effective method to improve both the corrosion resistance and consistency of magnesium alloys.

Keywords: Raw material purification; Mg; AZ31 magnesium alloy; Corrosion; Consistency of corrosion resistance.

1. Introduction

A key strategy to achieve "carbon peak and carbon neutrality" within the automobile industry is the implementation of lightweight technologies, which involves substituting traditional heavier materials with lighter alternatives, thereby reducing vehicle weight while preserving or enhancing performance, safety, and durability. Magnesium alloys emerge as particularly promising materials in this regard due to their low density (1.74 g$\cdot$ cm^{-3}), high strength-to-weight ratio (130 kNm$\cdot$ kg^{-1}), and recyclability. Among these, the AZ31 magnesium alloy is widely utilized for fuel car compressor housing, motor housing, and bracket parts, significantly reducing vehicle weight [1-3]. However, the broader application of AZ31 magnesium alloy in the automotive industry is currently hindered by its poor corrosion resistance. Analysis of the corrosion rates across various processing states of AZ31 magnesium alloy reveals substantial fluctuations in corrosion rates even within the same processing state (ranging from 0.4 to 215 mm $\cdot y^{-1}$ for as-cast alloy). Additionally, approximately 70 % of as-cast AZ31 magnesium alloy exhibits poor corrosion resistance (>1 mm $\cdot y^{-1}$, Corrosion resistance grade: Fair). Consequently, improving the corrosion resistance and ensuring the consistency of corrosion resistance properties in magnesium alloys are essential for expanding their application in the automotive industry.

The corrosion resistance of magnesium alloys is substantially affected by the presence of impurity elements, particularly iron (Fe), which has attracted considerable attention [4-9]. This is partly because the industrial melting of mag-

* Corresponding authors.
E-mail addresses: dg_xie@xjtu.edu.cn (D.-G. Xie), zwshan@xjtu.edu.cn (Z.-W. Shan).

https://doi.org/10.1016/j.jma.2024.10.018

Please cite this article as: X.-Y. Peng, D.-G. Xie, L.-Q. Bai et al., Enhanced corrosion resistance of AZ31 magnesium alloys through the use of high-purity raw magnesium, Journal of Magnesium and Alloys, https://doi.org/10.1016/j.jma.2024.10.018

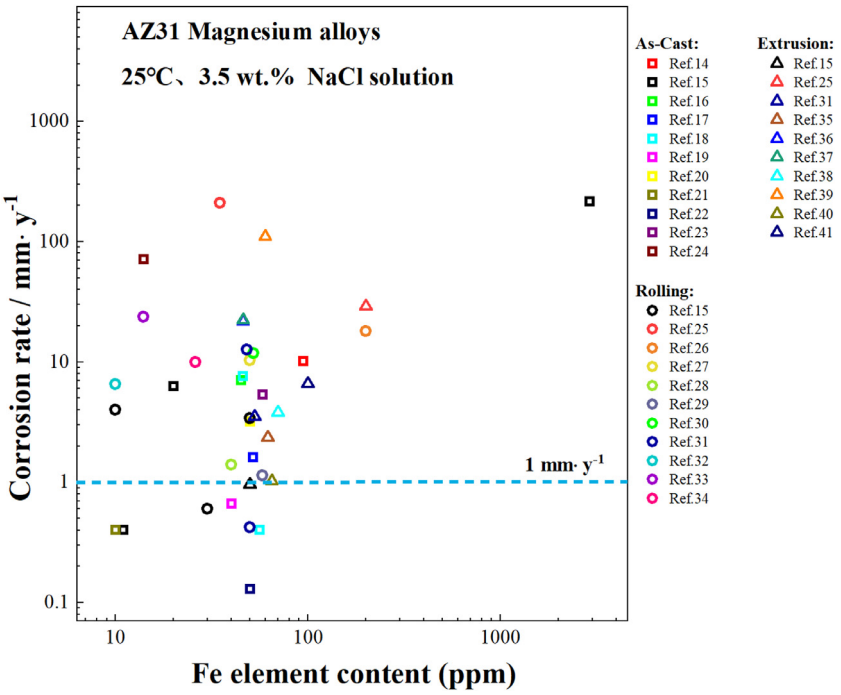

Fig. 1. Statistics of corrosion rates of AZ31 magnesium alloys with different Fe contents reported in Ref. [11–38].

nesium alloys typically occur in steel crucibles, making Fe contamination inevitable [10,11]. Additionally, extensive research has been conducted on how Fe impacts the corrosion resistance of magnesium alloys. Numerous studies demonstrated that the corrosion rate of magnesium alloys decreases rapidly with the reduction of Fe content, suggesting the existence of a critical threshold content for impurity elements in magnesium and its alloys, referred to as the corrosion tolerance limit [4,6-8,12,13]. When impurity content exceeds this limit, the corrosion rate substantially increases. For Fe, the corrosion tolerance limit in pure magnesium was reported to be 170 ppm [4,8,12], implying that the corrosion resistance should be good below that limit. However, other research indicates that in pure magnesium, the corrosion rates can still exceed 2 mm· y^{-1} even when Fe contents are below 50 ppm [13]. A systematic review of corrosion rates for AZ31 magnesium alloys in 3.5 wt.% NaCl solutions reveal significant fluctuations across a range of Fe contents [14-41] (Fig. 1), indicating no clear correlation exists between Fe contents and corrosion rates within the commonly observed ranges. Notably, substantial variations in corrosion rates persist even at Fe contents below 10 ppm. These results indicate that previous research might have overemphasized the influence of Fe while underestimating the impact of other impurities, which resulted in complex and fluctuating corrosion data without clear tendencies. Actually, these thoughts have been proposed as early as 1942 [4], which emphasis that the excellent corrosion resistance "is often masked because of the extreme sensitivity of these alloys to certain impurities and combinations of impurities". Therefore, Fe is not the only sensitive impurity element and not even the dominant one impacting the corrosion resistance of magnesium alloys. Other elements, such as Ni, Cu, Co, Si, Mn, etc., have also been reported to impact the corrosion resistance of magnesium alloys [4,6,7,42]. To enhance the corrosion resistance of magnesium alloys, it is essential to consider reducing the content of multiple impurities comprehensively rather than focusing exclusively on Fe reduction.

Generally, the impurities in magnesium alloy are either inherited from the raw magnesium or introduced during the alloying processes. Currently, in the industry, impurity content is mainly controlled through melt purification methods [43-46], which generally employ commercially pure magnesium and add fluxes or other additivity elements to the melt during melting to absorb or react with impurities, forming high-density compounds [45,46], thereby reducing impurity content by settling. While fluxes primarily remove nonmetallic impurities, specific metallic impurities require specific added elements. For AZ31 alloys, rare earth elements [42,44,47,48] or manganese (Mn) [42,45,47,49] have been added to remove Fe elements. However, this method cannot achieve a comprehensive reduction of impurity contents since these additives often target on a single or a few elements; meanwhile, these could also introduce other impurities. Subsequent corrosion tests have indicated that reducing the corrosion rate below 1 mm·y^{-1} is challenging using this approach [44,45]. Therefore, the widely adopted melt purification method makes it difficult to achieve a comprehensive reduction of impurities and, hence, it's not an effective approach to improving corrosion resistance.

Here we propose a potentially more direct and efficient approach to enhance corrosion resistance: raw magnesium purification, which employs high-purity raw magnesium for alloy preparation [50-52]. Previous research [50] has indicated that impurities from raw magnesium can be inherited into

Please cite this article as: X.-Y. Peng, D.-G. Xie, L.-Q. Bai et al., Enhanced corrosion resistance of AZ31 magnesium alloys through the use of high-purity raw magnesium, Journal of Magnesium and Alloys, https://doi.org/10.1016/j.jma.2024.10.018

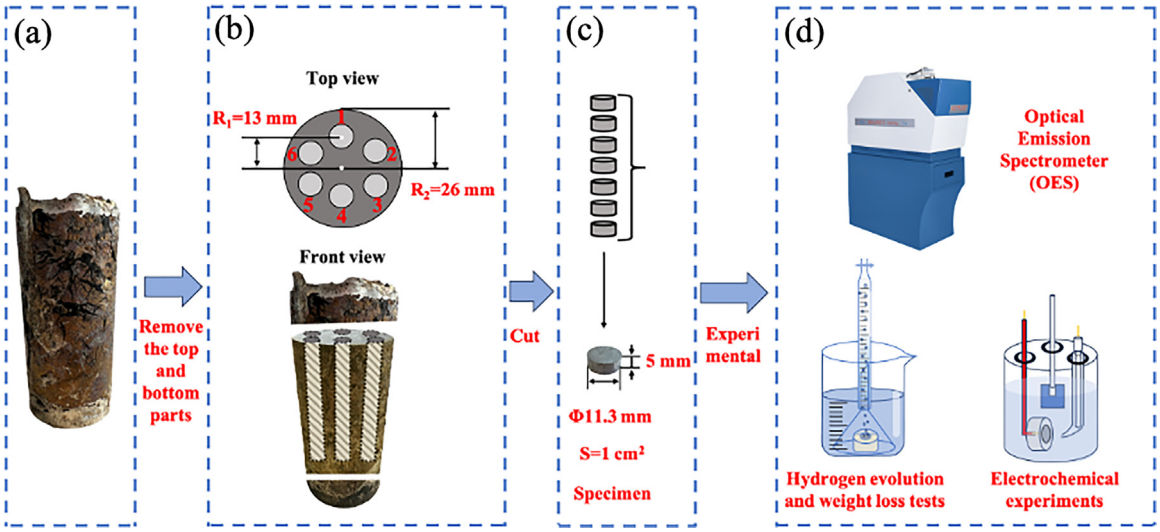

Fig. 2. As-cast AZ31 magnesium alloy ingot prepared by gravity casting method and the subsequent sampling process: (a) Image of the as-prepared ingot. (b) The illustration of the sampling position in the ingot. (c) The dimensions of the circular disk specimens. (d) The experimental of impurity content and corrosion tests.

magnesium alloys. The metal impurity content in commercial 99.9% (3N) pure magnesium is specified as ≤1000 ppm, whereas in 99.99% (4N) high-purity magnesium ≤100 ppm. Using 4N high-purity magnesium instead of 3N can achieve a comprehensive reduction of impurity content by roughly tenfold. Theoretically, alloys prepared from high-purity raw magnesium should have significantly reduced impurity content and enhance the corrosion resistance substantially. However, specific improvements in the corrosion resistance of AZ31 magnesium alloy prepared by higher-purity magnesium raw materials have yet to be reported. Therefore, this study aims to replace lower purity level raw magnesium (3N) with higher purity (4N) to investigate the content and distribution of impurity elements in AZ31 magnesium alloy and assess how reducing impurity content contributes to improved corrosion resistance and consistency.

2. Material and methods

2.1. Specimen preparation and chemical composition analysis

Pure Mg ingot with a purity of 99.9 % (3N) and high-purity Mg ingot with a purity of 99.99 % (4N) were used to prepare the AZ31 magnesium alloy. The resulting alloys were named AZ31–3N and AZ31–4N, respectively. During the ingot melting process, only Al and Zn with 99.99 % purity were added, excluding other elements, such as Mn, typically present in commercial AZ31 alloy. The ingots were prepared using the same melting process, which involved heating and melting material in a graphite crucible [10,11] under an Ar gas atmosphere. The actual ingots obtained are shown in Fig. 2.

In order to evaluate the consistency of composition and corrosion resistance of samples at different positions. The present adopts the following sampling method: remove the top and bottom of the ingot containing loose shrinkage and extract six test specimens for corrosion experiments and impurity detections only in the columnar crystal region of the ingot (approximately 1/2 of the ingot radius). The specific sampling process and location are shown in Fig. 2.

Table 1
Chemical composition of pure magnesium and AZ31 magnesium alloy (wt.%).

Alloy	Al	Zn	Mn	Fe	Si	Cu	Ni	Mg
Mg-3N	0.0085	0.0045	0.0150	0.0051	0.0140	0.0003	0.0002	Bal.
Mg-4N	0.0004	0.0015	0.0002	0.0011	0.0032	0.0001	0.0002	Bal.
AZ31–3N	3.5871	0.7450	0.0100	0.0064	0.0230	0.0002	0.0002	Bal.
AZ31–4N	3.4785	0.7310	0.0002	0.0006	0.0036	0.0001	0.0002	Bal.

The actual chemical compositions of the two raw magnesium and the two AZ31 alloys detected by inductively coupled plasma atomic emission spectrometry (ICP-AES) are shown in Table 1. In addition, the impurity concentration of the six test specimens was measured using optical emission spectroscopy (OES). Since the detection accuracy of OES is lower than that of ICP-AES, and significant differences in element contents between the alloy and the standard sample can result in less accurate detection values. Therefore, the OES data will deviate from the ICP-AES data. The OES data are shown in Fig. 3.

2.2. Corrosion tests

The corrosion rate of alloy specimens was measured by weight loss, hydrogen evolution, and electrochemical experiments, as shown in Fig. 2. All three corrosion testing methods were conducted in 3.5 wt.% NaCl solution at 25± 2 °C in an air-conditioned room.

Please cite this article as: X.-Y. Peng, D.-G. Xie, L.-Q. Bai et al., Enhanced corrosion resistance of AZ31 magnesium alloys through the use of high-purity raw magnesium, Journal of Magnesium and Alloys, https://doi.org/10.1016/j.jma.2024.10.018

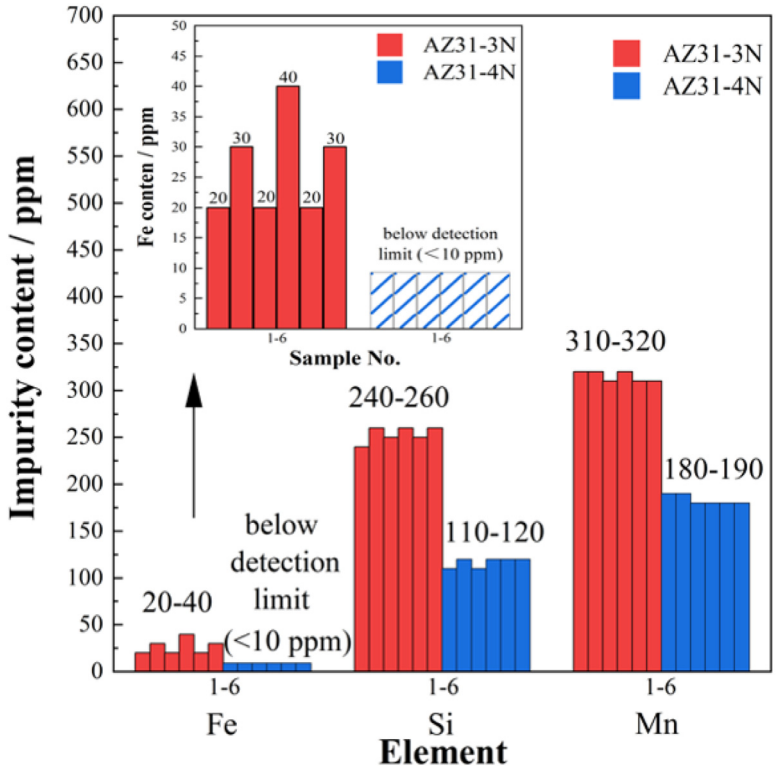

Fig. 3. Impurity content analysis of the 1–6 test points of two AZ31 magnesium alloys by optical emission spectrometer (OES). The main figure shows the content of the main impurity elements (Fe,Si,Mn) at each specimen. The small figure in the upper left corner shows the Fe impurity content.

Hydrogen evolution test allows the evaluation of both instantaneous and average corrosion rates. The hydrogen evolution rate, P_H (mm· y^{-1}), can be evaluated from the hydrogen evolution volume V_H (ml· cm^{-2}) and immersion time t (day) by the following Eq. (1) [8,53]:

$$P_H = 2.088V_H/t \quad (1)$$

Weight loss test is an average measurement over the whole immersion period. Weight loss and hydrogen evolution can be performed simultaneously, but corrosion rates measured by weight loss is generally higher than that measured by hydrogen evolution test [29]. The weight loss rate P*w* (mm· y^{-1}) is calculated from ΔW (mg· cm^{-2}· d^{-1}) according to the following equation [8,53]:

$$P_W = 2.10\Delta W \quad (2)$$

The electrochemical experiments measure the corrosion rate after a short period of specimen immersion. A standard three-electrode cell was adopted. The magnesium alloy served as the working electrode (WE), a Pt plate (20 mm × 20 mm × 1 mm) was the counter electrode (CE), and a saturated Ag/AgCl electrode acted as the reference electrode (RE). Potentiostats used were the French Bio-Logic multi-channel electrochemical workstation (VSP-300). The potentiodynamic polarization were measured in the range from E_{corr}+300 mV to E_{corr}-300 mV at a scan rate of 1 mV· s^{-1}. The corrosion current density, i_{corr} (μA· cm^{-2}) was estimated by Tafel extrapolation [8].

2.3. Microstructural characterization

The morphologies of the corroded surfaces of the two alloys were observed using an optical microscope and a scanning electron microscope (SEM, Hitachi SU8230) after the removal of corrosion products using a solution of 200 g· L^{-1} CrO_3 and 10 g· L^{-1} $AgNO_3$. The depth measurement of corrosion pits was performed using a confocal laser scanning microscope (CLSM, Leica DCM-8). The statistical analysis of corrosion areas was quantitatively analyzed using the Image J software, which segmented areas based on grayscale differences in the SEM images.

3. Results and discussion

3.1. The impurity contents and microstructures of two AZ31 alloys

The impurity contents of six specimens from AZ31–3N and AZ31–4N ingots, respectively, were measured using OES, as shown in Fig. 3. The major impurity elements in AZ31–3N alloy are Fe, Mn, and Si, with the content ranging from 20 to 40 ppm, 310–340 ppm, and 210–260 ppm, respectively. Other impurities were all below 10 ppm and could not be accurately detected due to it being smaller than the detection limit of OES used in this work. In contrast, the Fe content

Please cite this article as: X.-Y. Peng, D.-G. Xie, L.-Q. Bai et al., Enhanced corrosion resistance of AZ31 magnesium alloys through the use of high-purity raw magnesium, Journal of Magnesium and Alloys, https://doi.org/10.1016/j.jma.2024.10.018

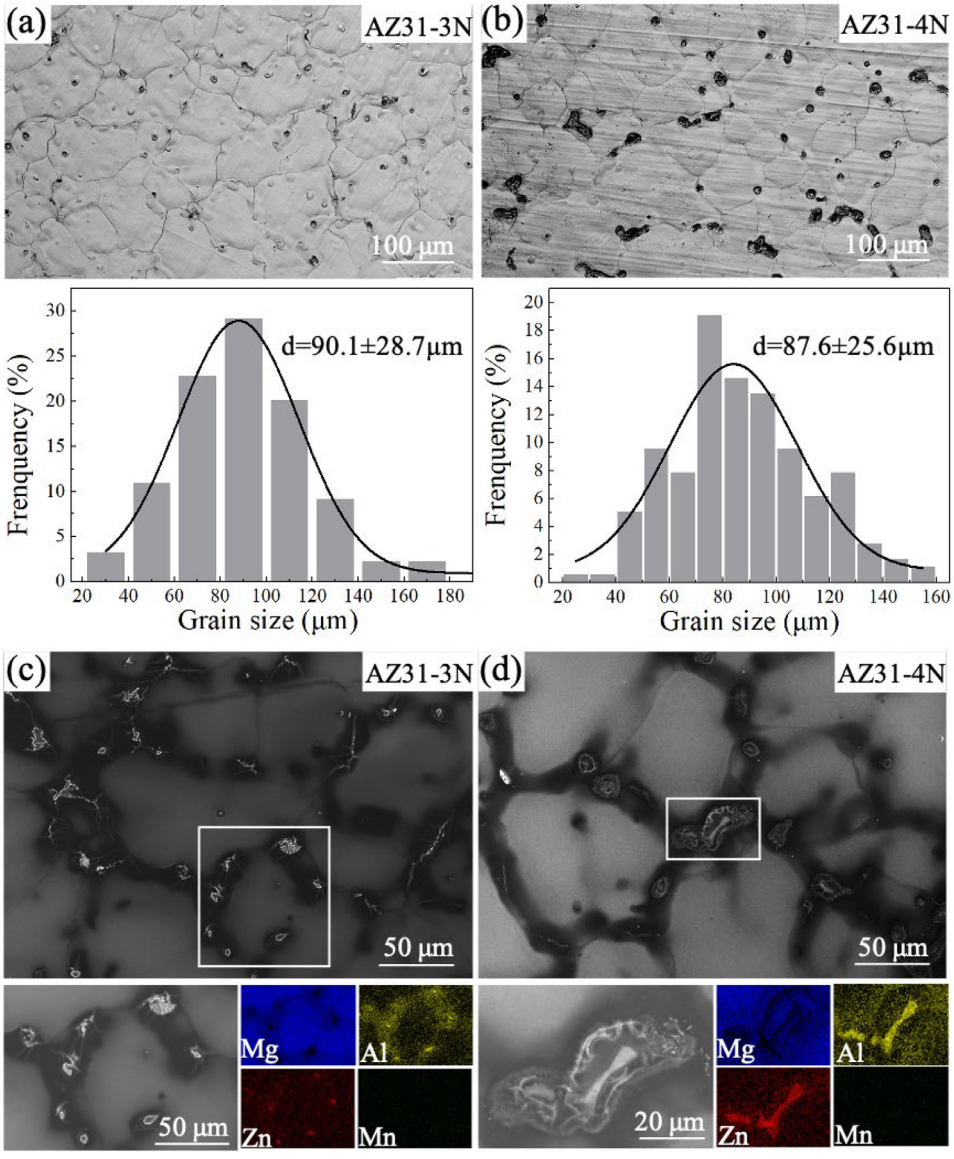

Fig. 4. Microstructure characterization of AZ31–3N and AZ31–4N magnesium alloys. (a-b) Optical micrographs showing the grain size distribution of AZ31–3N alloy and AZ31–4N alloy. (c-d) SEM micrographs and EDS maps showing the precipitation in AZ31–3N alloy and AZ31–4N alloy.

in AZ31–4N alloy was below the detection (10 ppm), which contrasts with the AZ31–3N alloy. In addition, the Mn and Si contents ranged from 180 to 190 ppm and 110–120 ppm, respectively, both lower than in AZ31–3N alloy. The contents of other impurities were also below 10 ppm. In AZ31–4N alloy, the content of all types of impurities has been substantially reduced than in AZ31–3N alloy, with Fe and Si reduced by approximately 66 % and 32 %, respectively. As well as the fluctuation range of impurity contents was also significantly reduced, particularly for Fe. The maximum fluctuation range of Fe in AZ31–3N alloy was 50 %, with the content differences up to 20 ppm, while in AZ31–4N alloy was <10 ppm. For Mn, Cu, Si, and Ni, the fluctuation range was about 5 % in AZ31–3N and about 2 % in AZ31–4N. These results indicate that using 4N high-purity magnesium instead of 3N pure magnesium can achieve a comprehensive reduction in both the impurity contents and their fluctuations in preparing AZ31 alloys.

Fig. 4 shows the optical and SEM micrographs of AZ31–3N and AZ31–4N alloys. The grain sizes of two alloys were counted from the optical micrographs and revealed that both alloys have comparable average grain sizes (~90 μm for AZ31–3N alloy and ~87 μm for AZ31–4N alloy). Additionally, the second phase in both alloys, identified as the β-$Mg_{17}Al_{12}$ phase through EDS mapping and appears with bright contrast in the SEM images in Fig. 4(c-d), displays similar discontinuous distribution along the grain boundary. No manganese-containing phases were detected, consistent with the absence of Mn additions during alloy fabrication.

Please cite this article as: X.-Y. Peng, D.-G. Xie, L.-Q. Bai et al., Enhanced corrosion resistance of AZ31 magnesium alloys through the use of high-purity raw magnesium, Journal of Magnesium and Alloys, https://doi.org/10.1016/j.jma.2024.10.018

3.2. The corrosion properties and the consistency of corrosion resistance

The corrosion resistance of two AZ31 magnesium alloys was evaluated using three experimental methods, as shown in Fig. 5. Fig. 5(a) shows the hydrogen evolution volume curves of AZ31–3N and AZ31–4N after immersion in 3.5 wt.% NaCl solution for 120 h. Initially, two alloys exhibited roughly similar hydrogen evolution behaviors for the first 10 h of immersion. However, with increasing immersion time, the hydrogen evolution volume of AZ31–3N alloy sharply increased. After 24 h, AZ31–3N alloy released 10 times more hydrogen evolution volume than AZ31–4N alloy. These results were consistent with the weight loss test, where AZ31–3N alloy also demonstrated obviously lower corrosion resistance compared with AZ31–4N alloy. Moreover, the corrosion rates were calculated for hydrogen evolution (P_H) and weight loss (P_W) according to Eq. (1) and Eq. (2), respectively, are shown in Fig. 5(b). For AZ31–3N alloy, the corrosion rates revealed P_H =39.75 ± 0.81 mm· y^{-1} and P_W =50.53 ± 3.57 mm· y^{-1}, whereas for AZ31–4N alloy, they revealed P_H =0.81 ± 0.07 mm· y^{-1} and P_W =2.11 ± 0.45 mm· y^{-1}, representing reductions of 98 % and 96 % compare to AZ31–3N alloy, respectively.

By analyzing the statistical dispersion of hydrogen evolution volume at each time point for AZ31–3N and 4N alloys, the consistency of corrosion resistance among the six specimens within two magnesium alloy ingots was assessed. Standard deviation served as the metric for assessing the consistency of corrosion resistance in the present work. As illustrated in Fig. 5(a), the error bars represent the standard deviation of hydrogen evolution volume for two AZ31 alloys. The AZ31–4N alloy exhibits minimal variation in error bandwidth, with values nearly overlapping the average value line. After 120 h, the total hydrogen evolution volume standard deviation was merely 0.07, indicating high consistency in corrosion resistance among the AZ31–4N specimens. In contrast, AZ31–3N alloy revealed a gradual increase in error bandwidth after 10 h, continuing up to 120 h, where the total hydrogen evolution volume standard deviation reached 0.81, reflecting significant variability in corrosion resistance. In summary, the range of corrosion resistance variation for AZ31–4N alloy is significantly reduced by 91 % compared with AZ31–3N alloy, demonstrating much higher consistency in corrosion resistance.

The open circuit potential (OCP) measurements of two AZ31 alloys were conducted prior to electrochemical impedance spectroscopy (EIS) and potentiodynamic polarization for 30 min, as shown in Fig. 5(c). The OCP curve of 4N alloy shows a continuous increase from −1.66 V to −1.56 V, while that of 3N alloy shows a rapid increase in the first 70 s and then a fluctuating plateau (−1.55 V). This contrast in the shape of OCP curves can be attributed to the formation of a much more stable corrosion product film on the 4N alloy surface than that on the 3N alloy surface [54]. In addition, Fig. 5(d) shows the potentiodynamic polarization curves of two alloys. The relevant data through Tafel fitting revealed that the corrosion current density (i_{corr}) of AZ31–4N magnesium alloy is 22.26 ± 6.92 μA·cm^{-2}, which is one order of magnitude lower than that of 3N alloy (i_{corr} = 143.12 ± 22.28 μA·cm^{-2}).

The Nyquist plots of electrochemical impedance spectroscopy (EIS) are depicted in Fig. 5(e). It shows that the 3N alloy exhibits a high-frequency capacitive loop followed by a low-frequency inductive loop. By contrast, the 4N alloy result is composed of no inductive loop but features two larger capacitive loops than that in 3N alloy result. According to the Baril's work, the presence of double capacitive loops feature indicates that the MgO / Mg $(OH)_2$ corrosion product layer formed on the 4N alloy surface is more stable and can effectively reduce the ionic diffusion through the surface layer [52,55-56]. In comparison, the 3N alloy experiences localized corrosion, the corrosion product film (MgO / Mg $(OH)_2$) on 3N alloy is less stable, thus is insufficient to hinder corrosion progression [39,57].

The equivalent circuits shown in Fig. 5(f-g) were used to fit the EIS results of AZ31–3N and AZ31–4N alloys, respectively. R_s is solution resistance, R_t and CPE_{dl} in parallel connection represent the charge transfer resistance and the capacitance of the electric double layer, respectively, R_t can reflect the difficulty of the corrosion process. R_L and L are inductor resistance and inductance. R_f and CPE_f are the resistance and the capacity of the corrosion product film, respectively. The fitted parameters are summarized in Table 2. The fitting results indicate that the R_f of AZ31–4N alloy is 1284 Ω•cm [2], representing effective protection from the surface film [52,55-56]. Additionally, the R_t of AZ31–4N alloy is an order of magnitude higher than that of AZ31–3N alloy, which is consistent with the higher dissolution rate of 3N alloy compared with 4N alloy. These three different test methods collectively demonstrate that the corrosion resistance of AZ31–4N alloy is substantially improved compared with AZ31–3N alloy.

3.3. Corrosion morphologies

The corrosion surface morphologies of AZ31–3N and AZ31–4N magnesium alloys immersed in 3.5 wt.% NaCl solution were illustrated in Fig. 6. Optical images (Fig. 6(a-b)) reveal distinct contrasts in the corroded surfaces after 120 h of immersion. The AZ31–3N alloy exhibited a very rough surface with severe corrosion in the entire surface and some localized corrosion sites. Notably, the two largest corrosion pits, outlined with red dashed rectangles in Fig. 6(a), have measured depths of approximately up to ~900 μm and 1600 μm, respectively. In contrast, AZ31–4N alloy only showed slight corrosion, maintaining a globally flat surface with silvery metallic luster and showing nearly no evidence of millimeter-scale corrosion pits. These macroscopic observations show that the corrosion of AZ31–4N alloy is substantially more uniform compared with AZ31–3N alloy. To reveal the microscopic origin of these differences in corrosion behavior, we performed SEM observation of two alloys after about 1 h of immersion in 3.5 wt.% NaCl solution when the corrosion only causes slight color change of the surfaces, as depicted

Please cite this article as: X.-Y. Peng, D.-G. Xie, L.-Q. Bai et al., Enhanced corrosion resistance of AZ31 magnesium alloys through the use of high-purity raw magnesium, Journal of Magnesium and Alloys, https://doi.org/10.1016/j.jma.2024.10.018

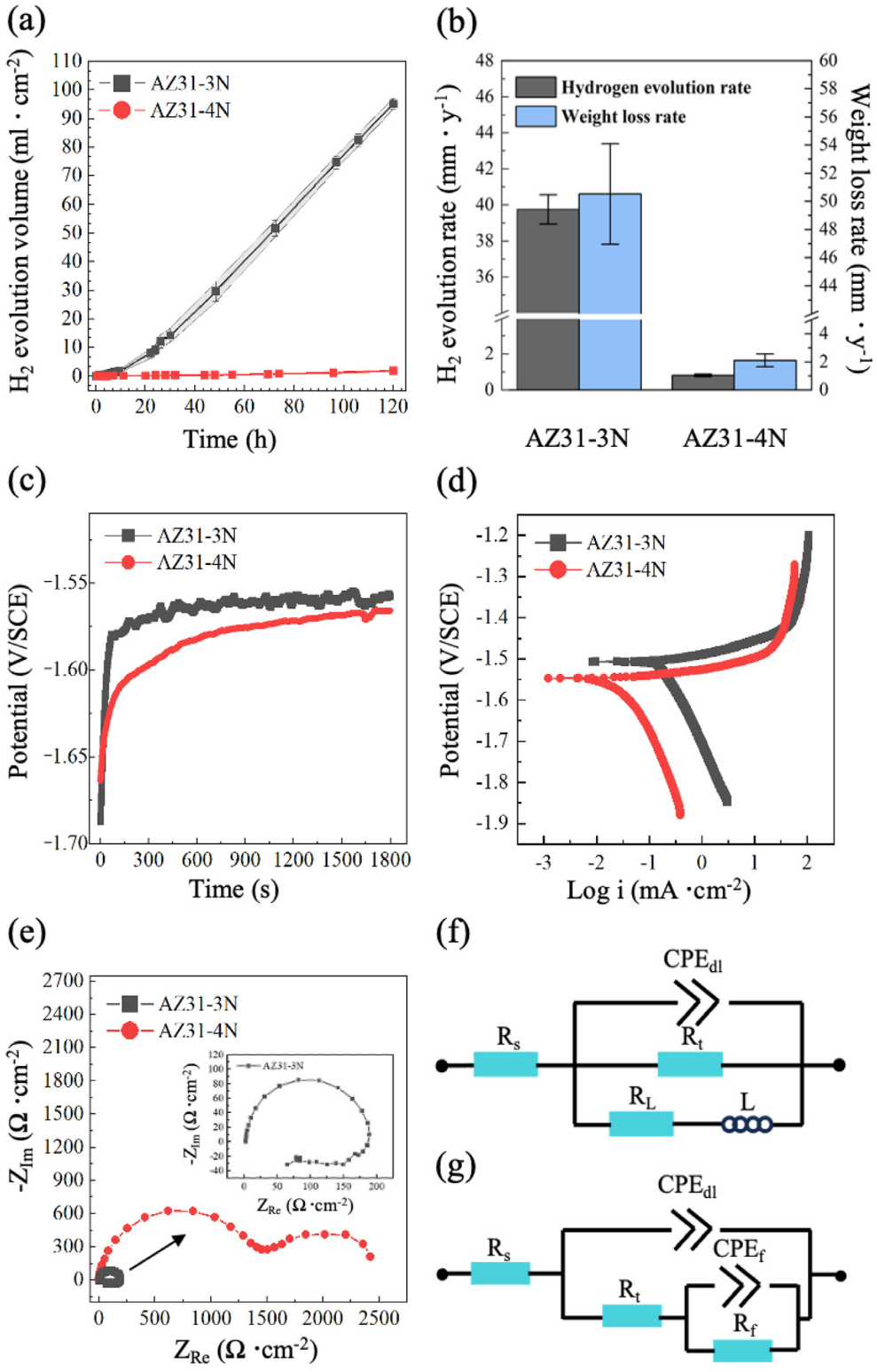

Fig. 5. Corrosion experiment of AZ31 magnesium alloys immersed in 3.5 wt.% NaCl solution: (a) Hydrogen evolution volume curves of two AZ31 magnesium alloys after immersion for 120 h, error bars are standard deviations and error bands are plotted (which can represent the change of corrosion resistance fluctuation at each time point). (b) Comparison of hydrogen evolution corrosion rate and weight loss corrosion rate. (c) Open circuit potential curves. (d) Potentiodynamic polarization curves. (e) Nyquist plots of electrochemical impedance spectroscopy (EIS). (f) and (g) are equivalent circuits for fitting the EIS spectrum of investigated AZ31- 3N alloy and AZ31–4N alloy, respectively.

Please cite this article as: X.-Y. Peng, D.-G. Xie, L.-Q. Bai et al., Enhanced corrosion resistance of AZ31 magnesium alloys through the use of high-purity raw magnesium, Journal of Magnesium and Alloys, https://doi.org/10.1016/j.jma.2024.10.018

Table 2
Fitting results of the EIS of AZ31 magnesium alloys.

	R_s, $\Omega\cdot cm^2$	CPE_{dl}, Y_0 $\Omega^{-1}\cdot cm^{-2}\cdot s^n$	n	R_t, $\Omega\cdot cm^2$	CPE_f, Y_0 $\Omega^{-1}\cdot cm^{-2}\cdot s^n$	n	R_f, $\Omega\cdot cm^2$	L $H\cdot cm^{-2}$	R_L, $\Omega\cdot cm^2$
AZ31-3N	1.9	1.7×10^{-5}	0.96	146.2	–	–	–	0.67	251.1
AZ31-4N	1.5	1.1×10^{-5}	0.98	1287	1.1×10^{-4}	0.67	1284	–	–

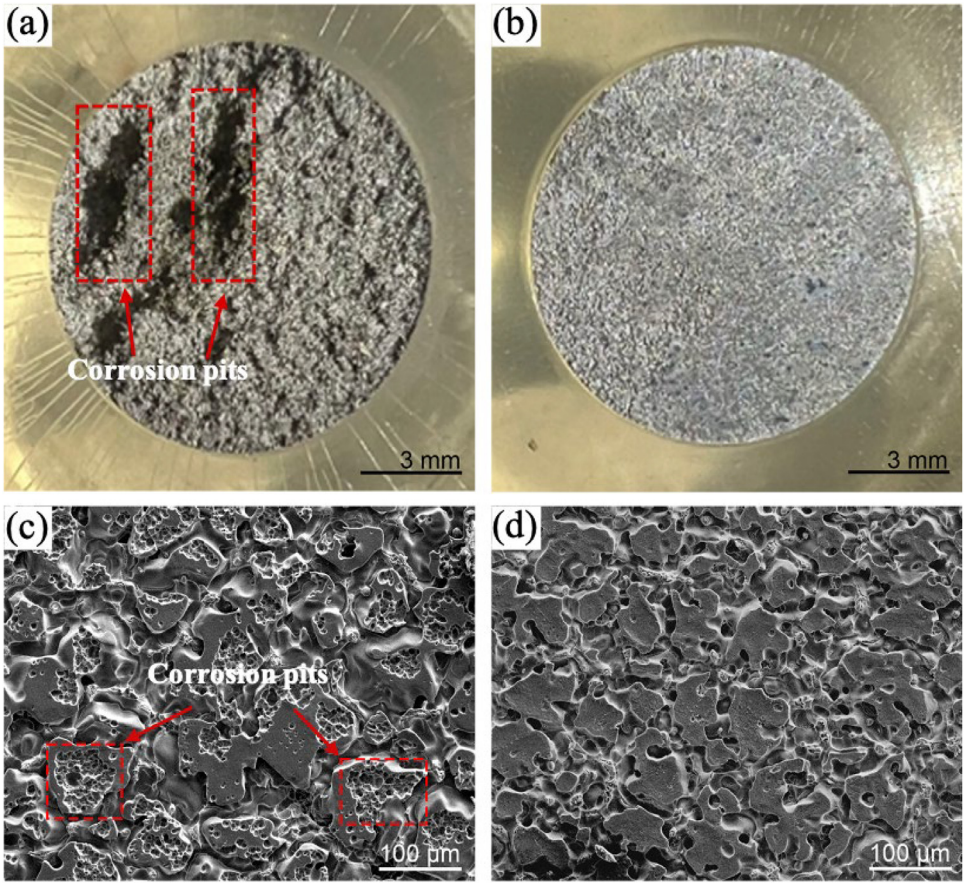

Fig. 6. Typical surface corrosion morphology of AZ31 magnesium alloys after immersion in 3.5 wt.% NaCl solution and the removal of corrosion products: (a-b) Comparison of macroscopic morphology of 3N and 4N magnesium alloys after immersion for 120 h (c-d) Comparison of microstructures of 3N and 4N magnesium alloys after immersion for 1 h. The dotted red line frame in (a) and (c) both shows the localized corrosion pits of 3N alloy.

in Fig. 6(c-d). In both alloys, the corrosion surfaces consist of network-shaped corrosion trenches and island-shaped plateaus, indicating that the dominant corrosion is along the grain boundary rather than the grain interior. However, there are two major differences between the two corrosion morphologies. The first is that AZ31–3N alloy had a rather large corroded area, occupying about 52 % of the total surface area, substantially higher than 36 % in the case of AZ31–4N alloy. These disparity in corroded areas is also manifested by the difference in the shape of corrosion trenches, which are narrower and shallower in AZ31–4N alloy compared with those in AZ31–3N alloy. Additionally, the large corrosion pits only appeared at the island-shaped plateaus of AZ31–3N alloy, indicative of severe pitting corrosion within the grains, as highlighted in Fig. 6(c). Conversely, AZ31–4N alloy exhibited tiny intragranular corrosion pits, indicating a more uniform corrosion morphology at the microscopic scale, as shown in Fig. 6(d). In conclusion, both macroscopic and microscopic analyses consistently indicate that AZ31–4N magnesium alloy exhibits more uniform corrosion and superior corrosion resistance compared with AZ31–3N alloy.

3.4. Discussion

The microscopic corrosion morphology of as-cast AZ31 alloy after immersion for 15 min is shown in Fig. 7(a-b), in both types of AZ31 magnesium alloys, corrosion preferentially occurred near the β-$Mg_{17}Al_{12}$ phase, which mainly distributed along the grain boundaries. According to previous reports [6,8,58] the β-$Mg_{17}Al_{12}$ phase can induce micro-galvanic corrosion with the neighboring α-Mg matrix, resulting in preferential corrosion near the grain boundaries.

Please cite this article as: X.-Y. Peng, D.-G. Xie, L.-Q. Bai et al., Enhanced corrosion resistance of AZ31 magnesium alloys through the use of high-purity raw magnesium, Journal of Magnesium and Alloys, https://doi.org/10.1016/j.jma.2024.10.018

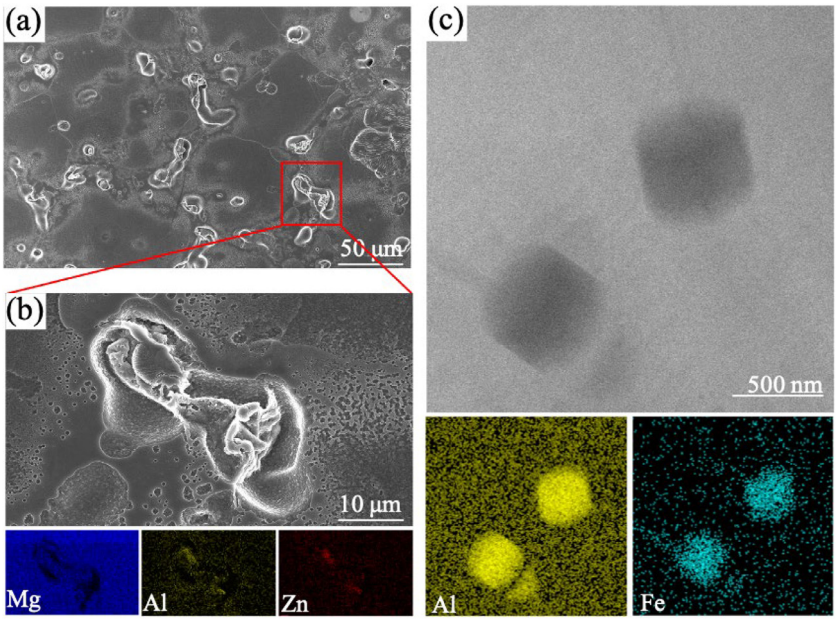

Fig. 7. The SEM micrographs, EDS maps, and TEM images of second phases in the studied alloys: (a-b) Surface corrosion morphology with EDS maps which is typical in both AZ31 magnesium alloys after immersion in 3.5 wt.% NaCl solution for 15 min and the removal of corrosion products; (c) TEM images of Al-Fe phase and elemental maps of Al, and Fe in AZ31–3N alloy.

However, both alloys contain approximately the same amount of the β-$Mg_{17}Al_{12}$ phases and the huge contrast in corrosion rates should have other origins, which could be attributed to the different content levels of impurity elements. Though multiple impurity elements have been reported to affect corrosion, the Fe element is the most studied and also the representative one that could drastically deteriorate the corrosion behavior. The Volta potential difference value of the Al-Fe phase is well known to be much higher than that of both the α-Mg matrix and the β-$Mg_{17}Al_{12}$ phase [52], which can accelerate the galvanic corrosion. Other precipitate phases may have similar roles in the corrosion behavior. Notably, Fe content in AZ31–3N alloy is 10 times higher than in AZ31–4N alloy. However, due to the extremely low impurity contents at the ppm level, characterizing the impurity distribution as solute atoms or as precipitates can be a great challenge. Fe usually exists as precipitation in Mg alloys [12,52], and by patiently searching multiple TEM samples, we fortunately located two Fe-rich particles only in studied AZ31–3N samples, as shown in Fig. 7(c). The two Fe-rich particles have diameters of ~500 nm and were confirmed with EDS elemental mappings. The existence of such Fe-rich particles can certainly increase the susceptibility to corrosion of AZ31–3N alloys. Furthermore, the fluctuation in Fe content within AZ31–3N alloy can reach up to 50 %, implying that the formation and distribution of precipitates may copy the same fluctuation. Thus, the presence of Al-Fe phase in AZ31–3N alloy is perhaps the main factor causing localized corrosion and resulting in a more ununiform corrosion morphology compared with that of AZ31–4N alloy. At last, we emphasize here that although we only experimentally characterized the Fe-rich particles, other impurity elements may also exist and distribute in different forms, potentially affecting the corrosion behavior. Therefore, it is reasonable to correlate the more severe and non-uniform corrosion in AZ31–3N alloy to its higher content and higher fluctuation of multiple impurity contents.

4. Conclusion

In this study, the corrosion resistance and consistency of as-cast AZ31 magnesium alloys with different impurity contents were prepared using two different purities of raw magnesium (3N and 4N). The results demonstrate that enhancing the purity of raw magnesium significantly reduces impurities in AZ31 alloys, with Fe and Si contents in AZ31–4N alloy decreasing by approximately 66 % and 32 %, respectively. This improvement leads to superior corrosion resistance and consistency. The corrosion rate of AZ31–4N alloy is 0.81 ± 0.07 $mm{\cdot}y^{-1}$, which is about 98 % lower than that of AZ31–3N alloy. Moreover, the fluctuation in the corrosion rate for AZ31–4N alloy is reduced by 91 %, indicating more uniform performance within the same ingot. Therefore, using raw magnesium with a higher purity level effectively reduces the content and uneven distribution of impurities such as Fe and Si, etc., resulting in AZ31 alloys with reduced non-uniform corrosion and enhanced more consistent corrosion resistance.

In this study, we emphasize the importance of considering both the absolute value and the fluctuation of corrosion rates when evaluating corrosion resistance. For magnesium alloys used in numerous structural applications, minimizing fluctuations in corrosion resistance is crucial. In additions, this study also offers novel insights into designing magnesium alloys with consistently low corrosion rates, addressing

Please cite this article as: X.-Y. Peng, D.-G. Xie, L.-Q. Bai et al., Enhanced corrosion resistance of AZ31 magnesium alloys through the use of high-purity raw magnesium, Journal of Magnesium and Alloys, https://doi.org/10.1016/j.jma.2024.10.018

a critical yet often underestimated aspect essential for broader industrial applications.

Declaration of competing interest

Zhiwei Shan is an editorial board member for Journal of Magnesium and Alloys and was not involved in the editorial review or the decision to publish this article. All authors declare that there are no competing interests.

CRediT authorship contribution statement

Xin-Yu Peng: Writing – original draft, Methodology, Investigation, Formal analysis, Data curation. **De-Gang Xie:** Writing – review & editing, Supervision, Methodology. **Long-Qi Bai:** Writing – review & editing, Formal analysis. **Zhang Liu:** Investigation, Formal analysis. **Zhi-Wei Shan:** Conceptualization, Supervision, Funding acquisition.

Acknowledgments

The authors gratefully acknowledge the support of the National Natural Science Foundation of China (52371122, 52031011), Shaanxi Province Foundation for Distinguished Young Scholars (2024JC-JCQN-47), and Shaanxi Province Science and Technology Department Project (2023ZSJD-05HZ).

References

[1] B. Liu, J. Yang, X.Y. Zhang, Q. Yang, J.S. Zhang, X.Q. Li, J. Magnes. Alloys 11 (2023) 15–47.
[2] H.Z. Yang, X.W. Yin, Y.F. Su, Z.Y. Wu, G. P, Auto Lightweig. 10 (2023) 56–59.
[3] H.C. Ji, Y.M. Li, H.Y. Long, W.C. Pei, Y.G. Li, Found. Technol. 040 (001) (2019) 122–128.
[4] J.D. Hanawalt, C.E. Nelson, J.A. Peloubet, Trans. AIME 147 (1942) 273–299.
[5] X.H. Chen, J.F. Wang, A.T. Tang, F.S. Pang, Materials Reports 24 (2010) 37–41.
[6] G.-L. Song, A. Atrens, Adv. Eng. Mater. 1 (1) (1999) 11–33.
[7] M. Esmaily, J.E. Svensson, S. Fajardo, N. Birbilis, G.S. Frankel, S. Virtanen, R. Arrabal, S. Thomas, L.G. Johansson, Prog. Mater. Sci. 89 (2017) 92–193.
[8] A. Atrens, M. Liu, N.I. Zainal Abidin, G. Song, in: G. Song (Ed.), Corrosion of Magnesium Alloys, Woodhead, Cambridge, (2011) 117–165.
[9] B. Shaw, Corrosion Resistance of Magnesium Alloys, ASM Handbook, 13 A, Corrosion: Fundamentals, Testing and Protection, 2003, pp. 692–696.
[10] L. Peng, G. Zeng, C.J. Lin, C.M. Gourlay, J. Alloys Compd. 854 (2020) 156415.
[11] P. Cao, Ma. Qian, D.H. StJohn, Scr. Mater. 51 (2) (2004) 125–129.
[12] M. Liu, P.J. Uggowitzer, A.V. Nagasekhar, P. Schmutz, M. Easton, G.-L. Song, A. Atrens, Corros. Sci. 51 (2009) 602–619.
[13] L. Yang, G.K. Liu, L.G. Ma, E.L. Zhang, X.R. Zhou, G. Thompson, Corros. Sci. 139 (2018) 421–429.
[14] C. Zhang, L. Wu, G.S. Huang, Y. Huang, B. Jiang, A. Atrens, F.S. Pan, J. Alloys Compd. 823 (2020) 153844.
[15] A. Atrens, Z.M. Shi, S.U. Mehreen, S. Johnston, G.-L. Song, X.H. Chen, F.S. Pan, J. Magnes. Alloy. 8 (4) (2020) 989–998.
[16] S.-M. Baek, S.-Y. Lee, J.C. Kim, J. Kwon, H. Jung, S. Lee, K.-S. Lee, S.S. Park, Corros. Sci. 178 (2021) 108998.
[17] X.G. Sun, M. Nouri, Y. Wang, D.Y. Li, Wear 302 (1–2) (2013) 1624–1632.
[18] Y. Chen, H. Yan, K.Z. Ji, L.S.B. Ling, C. Luo, R.L. Liu, Z. Hu, K. Li, Y. Xin, J. Electrochem. Soc 167 (16) (2020) 161505.
[19] X.L. He, Z.F. Yan, H.Y. Liang, R. Bai, Y.Z. She, 2020 Rare Metal Mat. Eng., 49 2997–3004.
[20] H.Y. Choi, W.J. Kim, J. Alloys Compd. 696 (2017) 736–745.
[21] S.Q. Yuan, M.Lu H, Z.G. Sun, L. Fan, X.Y. Zhu, W. Zhang, J. Electrochem. Soc 163 (2016) 7.
[22] K. Schlüter, C. Zamponi, A. Piorra, E. Quandt, Corros. Sci. 52 (12) (2010) 3973–3977.
[23] N.N. Aung, W. Zhou, Corros. Sci. 52 (2) (2010) 589–594.
[24] B. Jiang, Q. Xiang, A. Atrens, J.F. Song, F.S. Pan, Corros. Sci. 126 (2017) 374–380.
[25] H. Chen, J.W. Tang, W.W. Gong, Y.P. Gao, F. Tian, L. Chen, J. Mater. Res. Technol. 15 (2021) 4800–4812.
[26] D.S. Wei, J.G. Wang, Y. Liu, D.W. Wang, S.Y. Li, H.Y. Wang, Chem. Eng. J 404 (2021) 126444.
[27] B.Q. Chen, C. Xin, G.F. Zhang, F. Zhou, L.J. Zhang, J. Mater. Eng. Perform 28 (2019) 1253–1262.
[28] B.J. Wang, D.K. Xu, Y.C. Xin, L.Y. Sheng, E.H. Han, Sci. Rep 7 (1) (2017) 16014.
[29] M. Deng, L.Q. Wang, D. Höche, S.V. Lamaka, C. Wang, D. Snihirova, Y.M. Jin, Y.H. Zhang, M.L. Zheludkevich, Mater. Horizons 8 (2021) 589–596.
[30] M.P. Brady, D.N. Leonard, E.A. McNally, J.R. Kish, H.M. Meyer III, E. Cakmak, B. Davis, J. Electrochem. Soc. 166 (14) (2019) C492–C508.
[31] P.P. Wang, H.T. Jiang, Y.J. Wang, Y. Zhang, J.C. Tao, Acta Metall. Sin. Engl. Lett. 35 (2022) 941–947.
[32] U.M. Chaudry, A. Farooq, A. Malik, M. Nabeel, M. Sufyan, A. Tayyeb, S. Asif, A. Inam, A. Elbalaawy, E. Hafez, T.-S. Jun, K. Hamad, Mater. Technol. 37 (2022) 2230–2241.
[33] D.W. Li, H.Y. Wang, D.S. Wei, Z.X. Zhao, Y. Liu, ACS Omega 5 (2020) 1448–1456.
[34] W.T. Huo, W. Zhang, J.W. Lu, Y.S. Zhang, J. Alloys Compd. 720 (2017) 324–331.
[35] X. Li, B. Jiang, J.J. He, J.Y. Zhang, Z.T. Jiang, B. Liu, F.S. Pan, J. Alloys Compd. 721 (2017) 106–117.
[36] C. Zhang, L. Wu, G.S. Huang, K. Liu, B. Jiang, G.G. Wang, D.B. Xia, A. Atrens, F.S. Pan, J. Electrochem. Soc. 166 (13) (2019) C445–C453.
[37] R.L. Xin, B. Li, L. Li, Q. Liu, Mater. Des. 32 (8–9) (2011) 4548–4552.
[38] T.S. Lim, H.S. Ryu, S.-H. Hong, Corros. Sci. 62 (2012) 104–111.
[39] Q.Y. Xie, A. Ma, J.H. Jiang, H. Liu, Z.J. Cheng, Y.X. Gu, Corros. Sci. 192 (2021) 109842.
[40] P.P. Wang, H.T. Jiang, Y.J. Wang, Y. Zhang, S.W. Tian, Y.F. Zhang, Z.M. Cao, Int. J. Miner. Metall. Mater. 29 (2022) 1559–1569.
[41] Q.H. Zang, H.M. Chen, J. Zhang, L. Wang, S.J. Chen, Y.X. Jin, J. Mater. Res. Technol. 14 (2021) 195–201.
[42] B. Mingo, R. Arrabal, M. Mohedano, C.L. Mendis, R. Del Olmo, E. Matykina, N. Hort, M.C. Merino, A. Pardo, Mater. Des 130 (2017) 48–58.
[43] F.S. Pan, X.H. Chen, T. Yan, T.T. Liu, J.J. Mao, W. Luo, Q. Wang, J. Peng, A.T. Tang, B. Jiang, J. Magnes. Alloys 4 (2016) 8–14.
[44] J.I. Kim, H.N. Nguyen, B.S. You, Y.M. Kim, Scr. Mater. 162 (2019) 355–360.
[45] T. Chen, Y. Yuan, T.T. Liu, D.J. Li, A.T. Tang, X.H. Chen, R. Schmid-Fetzer, F.S. Pan, JOM 73 (2021) 892–902.
[46] W.J. Ding, in: Magnesium Alloy Science and Technology, Science Press, Beijing, 2007, pp. 47–59.
[47] S.Y. Jiang, L. Yang, Y. Yuan, L.G. Zhang, J. Wang, T. Chen, A.T. Tang, L.F. Ma, F.S. Pan, Metals (Basel) 13 (2023) 1466.
[48] Z. Zhang, J.S. Xie, J.H. Zhang, H. Dong, S.J. Liu, X.B. Zhang, J. Wang, R.Z. Wu, J. Mater. Sci. Technol. 150 (2023) 49–64.

Please cite this article as: X.-Y. Peng, D.-G. Xie, L.-Q. Bai et al., Enhanced corrosion resistance of AZ31 magnesium alloys through the use of high-purity raw magnesium, Journal of Magnesium and Alloys, https://doi.org/10.1016/j.jma.2024.10.018

[49] F.S. Pan, J.J. Mao, X.H. Chen, A.T. Tang, Z.W. Yu, Q. Wang, A Method to Increase the Purity of Magnesium Alloys By Mn Addition, China Patent, No. 201510042971.7, 2015-05-20. 2015.
[50] B. Yang, B.Y. Liu, H. Yang, Z.W. Shan, Materials China 39 (7) (2020) 576–584.
[51] Y.J. Li, T.J. Luo, Y.S. Yang, Trans. Nonferrous Met. Soc. China 20 (2010) s407–s410.
[52] S.K. Woo, B.-C. Suh, H.S. Kim, C.D. Yim, J. Magnes. Alloys 11 (2023) 851–868.
[53] ASTM G31-72, (2004).
[54] P.W. Chu, E.A. Marquis, Corros. Sci. 101 (2015) 94–104.
[55] G. Baril, C. Blanc, N. Pebere, Electrochem. Soc. 148 (12) (2001) B489–B496.
[56] G. Baril, N. Pebere, Corros. Sci. 43 (3) (2001) 471–484.
[57] Q. Liu, Q. Ma, G. Chen, X. Cao, S. Zhang, J. Pan, G. Zhang, Q. Shi, Corros. Sci. 138 (2018) 284–296.
[58] A. Pardo, M.C. Merino, A.E. Coy, R. Arrabal, F. Viejo, E. Matykina, Corros. Sci 50 (2008) 823–834.

Please cite this article as: X.-Y. Peng, D.-G. Xie, L.-Q. Bai et al., Enhanced corrosion resistance of AZ31 magnesium alloys through the use of high-purity raw magnesium, Journal of Magnesium and Alloys, https://doi.org/10.1016/j.jma.2024.10.018